Full Paper

Propellants, Explosives, Pyrotechnics

DOI: 10.1002/prep.201800069

Preparation and Performance of Pentaerythrite Tetranitrate-Based Composites by Direct Ink Writing

Chuanhao Xu,[a] Chongwei An,*[a, b] Qianbing Li,[a] Shuai Xu,[c] Shuang Wang,[a] Hao Guo,[a] and Jingyu Wang*[a, b]

Abstract: Direct ink writing (DIW), a promising technology for manufacturing energetic materials, has been a hot topic in the micro-scale charge of explosives. Herein, three kinds of pentaerythrite tetranitrate (PETN)-based all-liquid explosive inks were engineered and patterned using DIW. Scanning electron microscopy, energy-dispersive x-ray spectroscopy, X-ray diffraction, differential scanning calorimetry, and nanoindentation were used to characterize the printed samples. The density, thickness of single layer, impact sensitivity and critical size of detonation were measured and analyzed. Results show that PETN/EC/Viton exhibits excellent properties, specifically greater activation energy (148.09 KJ mol^{-1}), elastic modulus (2.808 GPa), and characteristic height (49.9 cm, 2.5 kg), over the two other samples. Moreover, a directly deposited sample in small grooves can provide steady detonation above the size of 1×0.101 mm. These features all contribute to the application of micro-size detonation to a certain degree.

Keywords: Direct ink writing (DIW) · pentaerythrite tetranitrate (PETN) · apparent activation energy · elastic modulus · impact sensitivity · critical size of detonation

1 Introduction

Direct ink writing (DIW) is a burgeoning technology that offers an attractive choice for manufacturing materials, including ceramics, sensors, microelectrodes, and engineered tissue, by enabling the creation of large area flexible devices at a low cost [1–4]. Meanwhile, DIW opens new avenues for the manufacture of energetic materials exhibiting excellent properties and flexible patterns. Relative to traditional charge styles such as casting and press in energetic materials, DIW is optimal for loading explosives in micro grooves and holes relying on its micro nozzle and flexible arm. In addition, the characterization of the required low pressure and temperature is important to ensure safety during the manufacture of explosive materials [5,6].

The preparation of printable explosive inks is essential to maximize the combination of DIW and explosive materials. Explosive inks reported in the literature can be classified into two structure types, namely, suspended and all-liquid. Suspended explosive ink require explosive particles to suspend in the liquid phase, whereas visible particles are absent in all-liquid explosive inks. Studies on explosive inks mainly focused on the suspended type. In 2010, a hexanitrohexaazaisowurtzitane (CL-20)-based secondary explosive ink, was developed for the DIW loading of micro electromechanical systems (MEMS) devices and qualified by the US Army for use as a booster explosive [5]. In 2013, Zhu reported a CL-20/PVA/EC/IPA/H_2O suspended explosive ink, whose critical size of detonation reached 0.54×0.36 mm [7]. In 2016, Wang designed a CL-20/GAP based formulation whose sample of direct write can steady detonate at 0.4×0.4 mm [8].

The preparation of suspended explosive inks is tedious because it involves the refinement of explosive materials, the preparation of a binder system, and the assembly of both. The formulation and printing of all-liquid explosive inks have obvious advantages because this type of ink is simply prepared by dissolving solutes into organic solvents, thereby removing the need for an additional processing step to produce printable inks. However, the development of all-liquid explosive inks is slow. Only Ihnen [9,10] explored the printed mechanism of pentaerythrite tetranitrate (PETN)- and cyclotrimethylenetrinitramine (RDX)- based explosive inks by an inkjet printer but did not characterize the properties of printed samples. In our previous work, we studied the CL-20-based all-liquid explosive ink [11], but CL-20 is restricted to its crystal transition during manufacture, which causes safety issues during applications. Thus, finding

[a] *C. Xu, C. An, Q. Li, S. Wang, H. Guo, J. Wang*
School of Environment and Safety Engineering
North University of China
Taiyuan Shanxi, 030051, P. R. China
**e-mail: anchongwei@yeah.net*
wjywjy67@163.com
[b] *C. An, J. Wang*
Shanxi engineering technology research centre for ultrafine powder
Taiyuan Shanxi, 030051, P. R. China
[c] *S. Xu*
SiChuan HuaChuan Industries Co., Ltd
Chengdu SiChuan, 610106, P. R. China

a suitable explosive with high energy and stability during manufacture is important.

PETN [$C(CH_2ONO_2)_4$], the nitrate ester of pentaerythritol, is an important crystalline energetic material that is extensively used as an ingredient in many high explosive formulations [12]. Compared with CL-20, PETN does not possess any advantages in crystal density and energy. PETN is a promising replacement in DIW because of its critical detonation size, which is reportedly smaller than that of CL-20, and this property contribute to the detonation transition in the micro size groove [13]. Moreover, crystal morphology of PETN is more steady than that of CL-20 during manufacture. These features render PETN a promising candidate used in all-liquid explosive inks. Nonetheless, the shortcomings of PETN in thermal sensitivity and impact sensitivity cannot be neglected. Thus, suitable binders should be searched.

Ethyl cellulose (EC) is a type of cellulose derivative that can form strong bonds with explosive materials in double-base propellants. Hence, EC has been utilized as a binder in suspended explosive inks with good performance [7, 14]. Viton, a popular binder with good thermal and mechanical property, has attracted considerable attention in plastic bonded explosives [14, 15]. In the present work, PETN was used as the main explosive in an all-liquid explosive ink with acetone as the solvent. EC and Viton were engineered as binders to form three binder systems, i was used as the printed samples was characterized and tested.

2 Experimental Section

2.1 Materials

Raw PETN with particle size ranged from 200–500 μm was provided by Shanxi Beihua Guanlv Chemical engineering co. LTD. (Yuncheng, China). EC was provided by Ningjin country xinda Chemical co. LTD. (Dezhou, China). Analytical reagent-grade (AR) Viton was obtained from Guangdong Mingju Plastic Industry Ltd. (Guangdong, China). Acetone, AR, was provided by Tianjin Fuchen chemical reagents factory. (Tianjin, China).

2.2 Preparation of PETN-Based Explosive Ink and Ink Patterning

Table 1 lists the three formulations of PETN-based explosive inks, whose preparation processes were exhibited in Scheme 1. All components, including raw PETN (15 %), binders (1.66 %) and acetone (83.34 %), were mixed in a beaker under ultrasonic oscillation for 5 min to produce an all-liquid explosive ink. Prior to printing, the ink was passed through a 25 μm nylon filter to remove any large, undissolved materials or other contaminants that may have inadvertently entered the ink. Then, the explosive ink was poured into the syringe of DIW platform [11], which consisted of a Nordson EFD piezoelectric printer nozzle and a three-axis motion platform produced by Xiamen TeYing Automation Technology Co. Ltd (Xiamen, China), and patterning was observed. The process flow diagram is shown in Scheme 1.

Table 1. Weight percentage of PETN-based explosive inks.

Formulations	Raw PETN (%)	EC (%)	Viton (%)	Acetone (%)
1	15	1.66	0	83.34
2	15	0.83	0.83	83.34
3	15	0	1.66	83.34

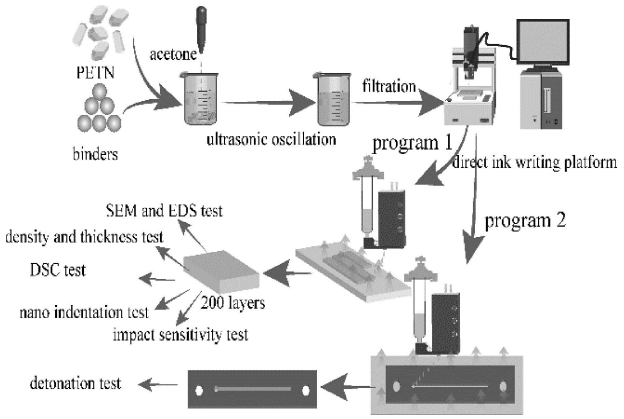

Scheme 1. Process flow diagram of direct ink writing.

Under the air pressure of 0.05 MPa, the all-liquid explosive ink was forced into the print head through which droplets were extruded out from a 0.1 mm-diameter nozzle to deposit onto a substrate in which the temperature was 40 °C to build a 3D structure in a layer-by-layer manner using the positioning stage in DIW. Two programs were established for adapting to different test requirements. Program 1 was designed to pattern a cub with 50 mm length, 7.5 mm width, and 200 layers, and the printed cub was utilized to characterize the density, layer thickness, particle size, polymorph, thermal decomposition properties, and impact sensitivity. Program 2 whose length was 100 mm and width was 1 mm was applied to fill the wedge groove channel of aluminium plate, which was used to measure the critical size of detonation [11]. During manufacture, the values of pulse and circulation that controlled the droplets volume extruded was set as 0.3 and 5.0 ms, respectively, to attain rapid prototyping. Moreover, the velocity of the robot arm in DIW was set as 50 mm s^{-1}, and the space between the nozzle and the substrate was 3 mm.

2.3 Characterization and Testing

The density of PETN-based composites was tested five times by a MZ-220SD electronic densimeter (Shenzhen city

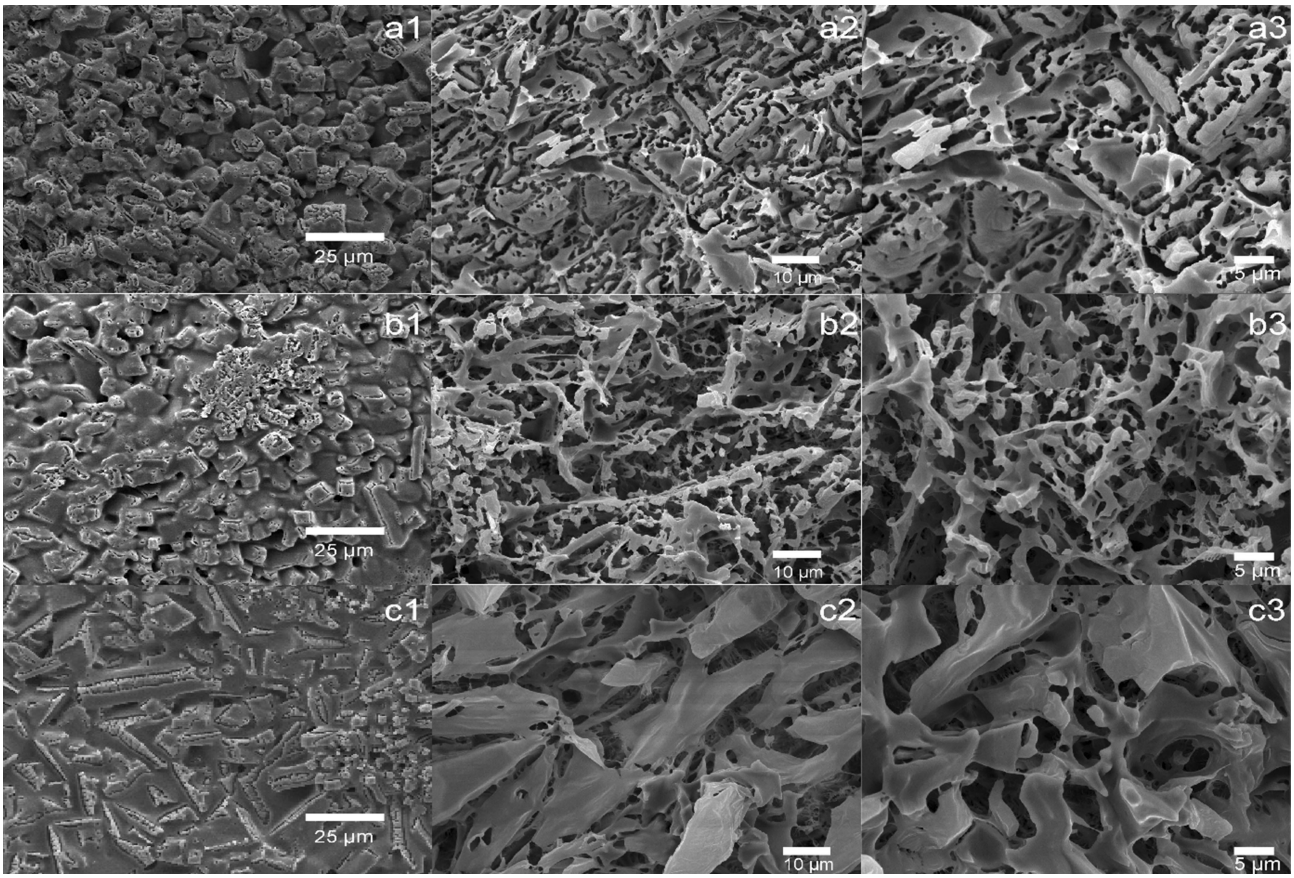

Figure 1. SEM photos of PETN-based printed samples: a1, b1 and c1 are the surface pictures of PETN/EC, PETN/EC/Viton and PETN/Viton, respectively; a2–3, b2–3 and c2–3 are the cross section pictures of PETN/EC, PETN/EC/Viton and PETN/Viton under different magnification time.

Tatsu letter Instrument Co., Ltd), and the mean value was determined. The surface and inner structure of PETN-based composites were observed via scanning electron microscopy (SEM, Mira 3, TESCAN, Brno, Czechia) with energy-dispersive x-ray spectroscopy (EDS, Oxford Instruments X-max 80, Concord, MA). The thickness of a single layer of composite was tested in the indirect approach, where the mean thickness of 200 layers was measured by a 44302-b digital microscope of Celestron. Morphology was identified by a DX-2700 X-ray diffraction (XRD) (Dandong HaoYuan Instrument Co., Ltd, Dandong, China) instrument. The properties of thermal decomposition were evaluated using a Setaram DSC131 instrument. Mechanical properties was tested by a Nano Indenter G200 with the Agilent NanoSuit software (Agilent Technologies Inc.).

Critical size of detonation was tested by loading the explosive ink into the wedge groove channel of the base plate made of aluminum. The groove length (A) in the base plate was 100 mm, the width was 1 mm, and the deepest side (C) was 3 mm. Then, the base plate was tightly fastened by cover plate and ignited by 8# detonators.

Impact sensitivity was surveyed by an ERL type 12 drop hammer apparatus. The testing conditions were drop weight of 2.500 ± 0.002 kg, sample mass of 35 ± 1 mg, and room temperature. The results were expressed by the critical drop height of 50% explosion probability (H_{50}) and standard deviation (S).

3 Results and Discussion

3.1 SEM Photos and EDS Analysis

SEM was employed under different magnification times to study the surface morphology and inner structures of the printed samples. The images of a1, a2 and a3 (Figure 1) show the surface of the printed samples in accordance with formulations 1 (PETN/EC), 2 (PETN/EC/Viton), and 3 (PETN/Viton) in Table 1 respectively. Cross-sectional images of PETN/EC, PETN/EC/Viton and PETN/Viton are displayed in a2–3, b2–3, and c2–3 in Figure 1, respectively.

Many particles 5–20 μm in size are uniformly distributed in a1 of Figure 1, and the diameter of voids and holes is ap-

proximately 5 μm. The smoothness of c1 is similar to that of a1, but their structure and particles are different. Separately, b1 does not integrate the two advantages of a1 and c1, although the binders used are the combination of EC and Viton. However, the granule size is consistent with a1. The cross-sectional images illustrate that all samples possess voids and holes, which are related to the rapid evaporation of solvent. During manufacture, air fills the composites when acetone evaporates [16].

In the cross section, b2 exhibits a large number of spherical particles with a size of approximately 1 μm. Compared with the particles in b2, the particles in a2 are smaller and fewer, whereas visible particles are absent in c2. The inner structures of a2 and c2 are laminated, whereas that of b2 is net like. These phenomena can be explained by the binary system of binders. During preparation, EC and Viton first precipitated from solution along with the volatilization of acetone and then grew to form a steady structure, where the two binders generate crosslinking and restrictions in each other, offering enough time and space for the growth of PETN crystals. As a result, large particles and voids are produced.

PETN comprises nitrogen element, and Viton has the particular element of fluorine. Thus, EDS can be used to further probe the inner structures of the printed samples. As shown in Figure a3 and a4, nitrogen and fluorine are well distributed, which indicated that PETN and Viton were also well distributed in the samples. Interestingly, obvious distinctions can be observed between b3 and b4 in Figure 2. A possible explanation is that PETN in the PETN/EC/Viton system may form a composite with EC and Viton as shown in a1 of Figure 2, but the existence form of PETN and Viton in the PETN/Viton composite is possibly similar to that in the physical mixture.

3.2 Density, Thickness of Single Layer and XRD Analysis

The average density (±0.01 g cm^{-3}) of PETN/EC, PETN/EC/Viton, and PETN/Viton are 1.43, 1.27 and 1.40 g cm^{-3}, respectively. Their corresponding theoretical maximum density (TMD) are 1.668, 1.724 and 1.755 g cm^{-3}. Thus, the ratio between the printed density and TMD in PETN/EC, PETN/EC/Viton, and PETN/Viton are 86.09 %, 73.92 %, and 78.74 %, respectively. This result is mainly due to the voids and holes in their inner structures, as shown in a2, b2, and c2 of Figure 1, where b2 has more obvious cracks than a2 and c2. In terms of energy, PETN/EC may possess the best capability among all samples, whereas PETN/EC/Viton is likely to be the worst. However, the selection of energetic complex is not only limited to energy. Thus, a further study on other properties and performance should be researched.

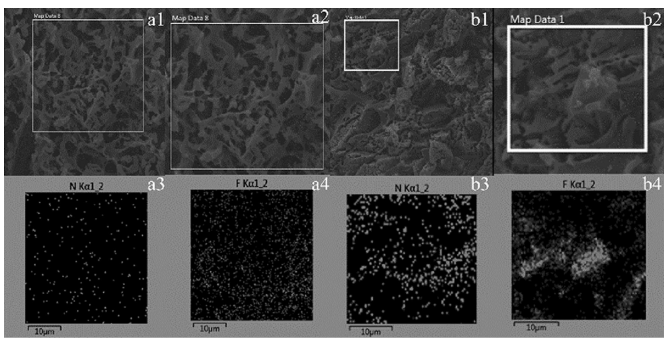

Figure 2. SEM and EDS patterns of cross section: a1–4 belong to PETN/EC/Viton, while b1–4 are PETN/Viton.

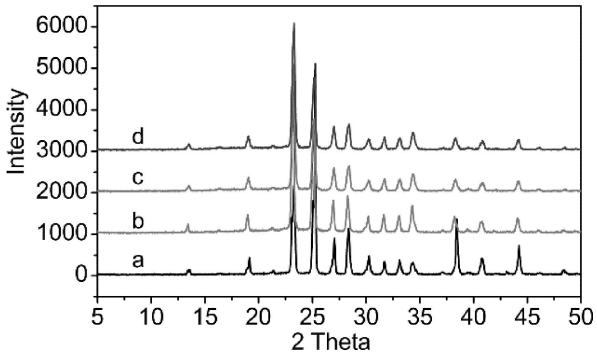

Figure 3. XRD pattern of raw PETN and PETN-based printed samples: a, b, c and d are raw PETN, PETN/EC, PETN/EC/Viton and PETN/Viton, respectively.

Owing to the printed manner of DIW, the singly-layer thickness during manufacture may not be uniform due to the small differences generated by heat conduction. Thus, indirect means was applied by testing the average thickness of 200 layers in the printed samples, whose value were 0.77, 0.62, and 0.72 mm, respectively. The average thickness single-layer in PETN/EC, PETN/EC/Viton and PETN/Viton are 3.85, 3.1 and 3.6 μm, respectively. This rule is consistence with the variation regulation of printed density. A possible explanation is that less layers in the composite bring fewer voids, which mainly exist in the connective positions, and the voids are the major factor affecting printed density. This speculation can be proved by the cross-section images in Figure 1.

Another important issue for explosive materials in weapon systems is the formation of crystal polymorphs. Thus, XRD was utilized with angles ranging from 5° to 50°, a step angle of 0.03, and a test temperature of 20 °C to distinguish the crystal form of PETN in the printed samples. As shown in Figure 3, the main diffraction angles in the curves of PETN/EC (b), PETN/EC/Viton (c), and PETN/Viton (d), such as 23.12°, 25.02°, 28.24° and 34.21°, which corresponded to the crystal faces of (201), (211), (102), and (212) of PETN, are consistent with raw PETN (a), indicated that DIW does not affect the crystal morphology of PETN.

3.3 Thermal Decomposition Properties and Calculation of Kinetic Parameters

Thermal property is one of the main factors in the use of explosive materials. Compare with nitramine explosive, PETN has high thermal sensitivity, which is one of the main factors restricting its use in ammunitions [17]. Thus, the thermal stability of PETN-based composites should be increased. In the present work, DSC was utilized to study the thermal decomposition of raw PETN and PETN-based printed samples under N_2 atmosphere with a flow rate of 20 ml min^{-1}.

Compared with that of raw PETN, the most exothermic peak temperatures of PETN-based composites decrease to a certain degree except at the heating rate of 5 K min^{-1} (Figure 4).Given that the heating rate of 5 K min^{-1} is not that fast, the thermal decomposition of binders would entail high heat cost, which causes a delay in exothermic peak temperature. As for the reduction in exothermal temperature at the heating rate of 10, 15 and 20 K min^{-1}, the reason can be attributed to the high surface energy at micro diameters [18].

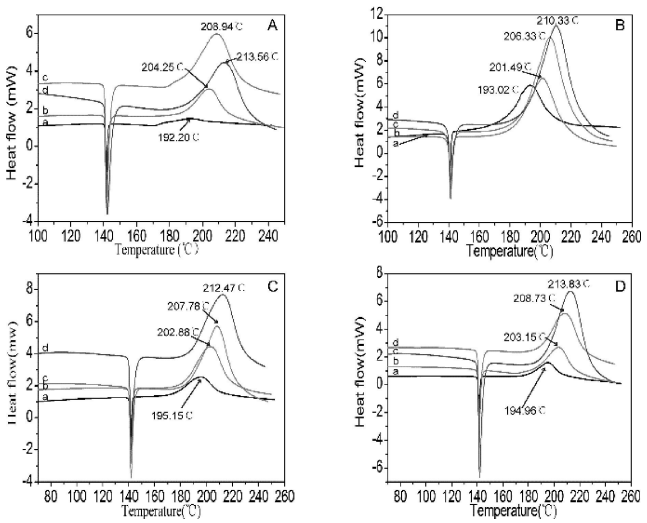

Figure 4. DSC curves of raw PETN and PETN-based printed samples: a, b, c and d are the curves at the heating rates of 5, 10, 15 and 20 K min^{-1}, respectively. A is raw PETN, B is PETN/EC, C is PETN/EC/Viton and D is PETN/Viton, respectively.

Kissinger's method [19], Ozawa's method [20], and Starink's method [21] have widely been used to determine the Arrhenius equation.

$$\ln\left(\frac{\beta}{T^s}\right) = -\left(\frac{BE}{RT}\right) + C \quad (1)$$

Where T is the peak temperature in K. E is the apparent activation energy in KJ mol^{-1}. R is the gas constant (8.314 J K^{-1} mol^{-1}). β is the linear heating rate in K min^{-1}, and B and C are constants. When s = 2 and B = 1, the equation is based on Kissinger's method. When s = 0, B = 1.0516, the equation is based on Ozawa's method. When s = 1.8 and B = 1.0037, the equation is based on Starink's method.

The apparent activation energy E can be calculated based on the linear relationship of ln(β/Tp^2), ln(β/Tp$^{1.8}$) and ln(β) to 1/Tp, which correspond to Kissinger's method, Ozawa's method, and Starink's method. The values are shown in Table 2, where R represents the linear correlation coefficient.

Table 2. Chemical kinetics parameters of raw PETN and PETN-based printed samples.

Samples	E (KJ mol^{-1}) K[a], R	O[b], R	S[c], R	average value	T_b(°C)
Raw PETN	114.64, 0.9871	122.54, 0.9886	115.43, 0.9873	117.54	180.38
PETN/EC	143.11, 0.9994	151, 0.9995	143.9, 0.9994	146	190.63
PETN/EC/Viton	145.19, 0.9924	153.11, 0.9933	145.98, 0.9925	148.09	194.19
PETN/Viton	132.53, 0.9908	140.47, 0.9919	133.33, 0.9909	135.44	195.83

[a] Kissinger's method. [b] Ozawa's method. [c] Starink's method.

The values of the peak temperature corresponding to β approaches 0 can be obtained from Equation (2), where a, b and c are coefficients [22].

$$T_{pi} = T_{p0} + a\beta + b\beta^2 + c\beta^3 \quad (2)$$

The corresponding critical temperatures of thermal explosion (Tb) can be calculated by Equation (3), where R is the gas constant and *E* is the value of E by Kissinger's method [21].

$$T_b = \frac{E - (E^2 - 4ERT_{p0})^{1/2}}{2R} \quad (3)$$

As shown in Table 2, the average apparent activation energies of PETN/EC, PETN/EC/Viton, and PETN/Viton exceed that of raw PETN by 28.46, 30.55, and 17.9 KJ mol^{-1}, respectively. This phenomenon illustrates that EC and Viton contribute to obtaining a PETN-based composite with higher thermal stability, and their combination shows the best performance among the samples. The values of raw PETN, PETN/EC, PETN/EC/Viton and PETN/Viton in critical temperatures of thermal explosion gradually increase to 180.38 °C, 190.63 °C, 194.19 °C, and 195.83 °C, respectively, implying that the addition of binders in PETN reduces thermal sensitivity and thus increases thermal stability. On average,

PETN/EC/Viton is the optimal choice for attaining a composite with good thermal stability.

3.4. Elastic Modulus and Hardness

Elastic modulus, a bridge between microstructure and macro-performance, is an importance mechanical parameter in printed samples. From the macro perspective, elastic modulus reflects the specific relationship between stresses and strain. Moreover, reflects the intermolecular forces between each component and the components on the micro level [23].

In the presented work, static loading model of Nano Indenter G200 with loading stress ranging from 0 to 500 mN was used to capture the mechanical behaviors of the PETN-based composites, and the tip type was wedge. Agilent NanoSuit was used to extract the elastic modulus and hardness. Every sample was tested five times, and the average value was obtained.

The indentation depth under maximal load is ranked in the order PETN/Viton (22,680.23 nm) < PETN/EC/Viton (22,863.68 nm) < PETN/EC (35,085.41 nm). This order corresponds to the average hardness values in Figure 5, suggesting that the addition of EC in the PETN-based complex can more effectively increase the rigidity than Viton.

The average elastic moduli of PETN/EC, PETN/EC/Viton and PETN/Viton shown in Figure 5 are 2.234, 2.808 and 2.326 GPa, respectively. This result indicates that PETN/EC/Viton has the best capability to resist external force among the three samples and that PETN/EC/Viton dose not easily generate deformation under external force. The differences between PETN/EC and PETN/Viton in this property mainly depend on the inner structure as shown in Figure 1. The diversity among those samples may be attributed to the effect of cooperative strengthening [24]. A small gap exists between PETN/EC and PETN/Viton, whereas the value of

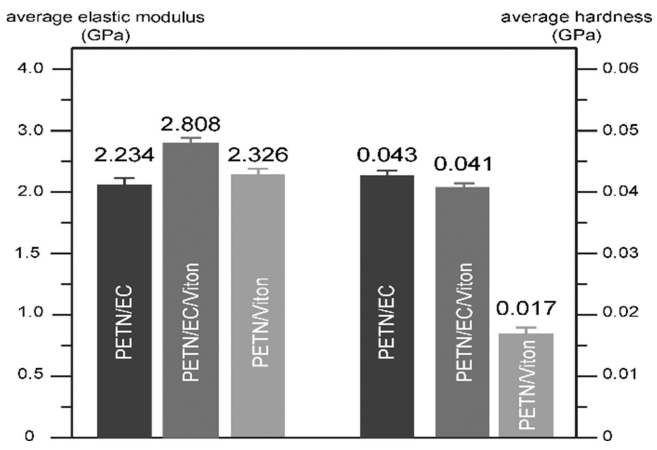

Figure 5. Average elastic modulus and hardness of PETN-based printed samples.

PETN/EC/Viton are binary complexes while PETN/EC/Viton is a ternary complex, the cooperative strengthening in the PETN/EC/Viton system is higher than that in the others. Correspondingly, the intermolecular force is stronger and the elastic modulus is higher in the ternary complex than in the other systems.

3.5 Impact Sensitivity Test and Critical Size of Detonation Test

Compared with that of raw PETN, the H_{50} values of the PETN-based composites (Table 3) increase by 21.1, 31.2 and 19.7 cm, respectively. This phenomenon may be attributed to the fact that binders reduce the friction between PETN particles, thereby reducing stress concentration, and also partially absorb heat, thereby preventing self-heating of the PETN to a certain extent [8, 25]. Binary binders perform better than individual ones, indicating that PETN/EC/Viton has the best impact safety among the samples.

Table 3. Impact sensitivity of raw PETN and PETN-based printed samples.

Samples	Impact Sensitivity[$H_{50}(\pm S)$]/cm		
	Experiment 1	Experiment 2	Average
raw PETN	18.8(±1.1)	18.6(±1.0)	18.7
PETN/EC	39.6(±0.8)	39.9(±1.2)	39.8
PETN/EC/Viton	49.7(±0.9)	50.0(±1.1)	49.9
PETN/Viton	38.2(±0.6)	38.6(±0.8)	38.4

To satisfy the demands of detonation at micro channel, the printed samples should have a suitable critical size of detonation (dc), whose value determines the minimum scale of grooves in the pyrotechnics system. In general, a compound with the lowest d_c value possible is preferred in the pyrotechnics system and conforms to the trend of military devices. Herein, explosive trace in the base plates after detonation was used to calculate the critical size of detonation by Equation (4) [11].

$$d_c = \frac{A - B}{A} \times C \quad (4)$$

where A is the length of charge, B is the explosion track, C is the bottom depth of wedge groove, and d_c is the critical size of detonation.

Figure 6 indicates that the B values of PETN/EC, PETN/EC/Viton, and PETN/Viton are 96.4, 96.33 and 96.62 mm, respectively. The values of A and C is known for 100 and 3 mm, respectively. Thus, the critical size of detonation in PETN/EC, PETN/EC/Viton, and PETN/Viton are calculated using Equation (4) to be 1×0.108, 1×0.101, and 1×0.140 mm. This result shows that PETN/EC/Viton has better

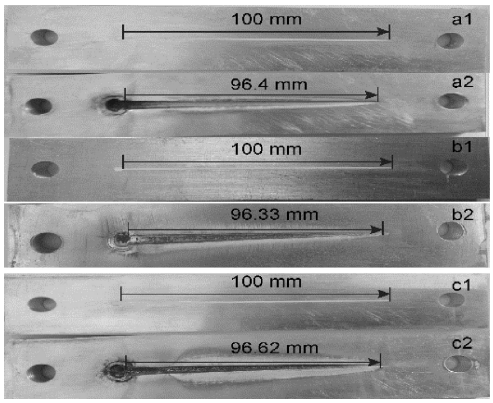

Figure 6. Pictures of base plates before and after detonation: a1–2, b1–b2 and c1–2 are PETN/EC, PETN/EC/Viton and PETN/Viton, respectively.

capability for stable detonation under micro size than PETN/EC and PETN/Viton.

Many black residues exist in the grooves of b2 and c2 in Figure 6, whereas a2 is very clean. EC always serves as an inhibitor, which should have desirable thermal and ablative characteristics such as high effective heat of ablation, ability to form a stable char, and self-heating characteristics [15], whereas Viton is a high-polymer elastomer. Thus, the black residues may be ascribed to the inadequate combustion of Viton.

4 Conclusions

Three PETN-based all-liquid explosive inks were processed with the assistance of DIW technology, and the performance of printed samples were characterized and tested. The inner structures of PETN/EC and PETN/Viton are laminated, whereas that of PETN/EC/Viton is net like. The particles in PETN/EC/Viton are spherical with sizes approximately 1 μm. The change rule of printed density is consistence with the regulation of the single-layer thickness. XRD patterns illustrate that DIW does not affect the crystal morphology of PETN. Among the three samples, PETN/EC/Viton shows the best thermal stability, impact safety, mechanical property and detonation stability, rendering it a promising candidate in the charge of micro grooves. This study may serve as a reference for further research on all-liquid explosive inks, and the presented DIW processing method can be extended to other explosives and binders.

Acknowledgements

This work was supported by the Advantage Disciplines Climbing Plan of Shanxi Province.

References

[1] J. A. Lewis, J. E. Smay, J. Stuecker, J. Cesarano, Direct Ink Writing of Three Dimensional Ceramic Structures, *J. Am. Ceram. Soc.* **2006**, *89*, 3599–3609.

[2] P. Sjoberg, A. Maattanen, U. Vanamo, M. Novell, P. Ihalainen, F. J. Andrade, J. Bobacka, J. Peltonen, Paper-Based Potentiometric Ion Sensors Constructed on Ink-jet Printed Gold Electrodes, *Sens. Actuators, B.* **2016**, *224*, 325–332.

[3] B. Y. Ahn, E. B. Duoss, M. J. Motala, X. Y. Guo, S. I. Park, Y. J. Xiong, J. Yoon, R. G. Nuzzo, J. A. Rogers, J. A. Lewis, Omnidirectional Printing of Flexible, Stretchable, and Spanning Silver Microelectrodes, *Science.* **2009**, *323*, 1590–1593.

[4] S. Ghosh, S. T. Parker, X. Y. Wang, D. L. Kaplan, J. A. Lewis, Direct Write Assembly of Microperiodic Silk Fibroin Scaffolds for Tissue Engineering Applications, *Adv. Funct. Mater.* **2008**, *18*, 1883–1889.

[5] A. Ihen, W. Lee, B. Fuchs, A. Petrock, P. Samuels, V. Stepanov, A. D. Stasio, Inkjet-Printing of Nanocomposite High-Explosive Materials for Direct Write Fuzing, *54th Fuze Conference*, Kansas City, MO, USA, May **2010**, pp. 11–13.

[6] J. L. Zumino III, D. P. Schmidt, A. M. Petrock, B. E. Fuchs, Inkjet Printed Devices for Armament Applications, *NSTI-Nonotech.*, Anaheim, CA, USA, June, **2010**, 542–545.

[7] Z. Zhu, C. Jin, Z. Qiao, B. Huang, G. Yang, F. Nie, Preparation and Characterization of Direct Write Explosive Ink Based on CL-20, *Chin. J. Energ. Mater.* **2013**, *21*, 235–238.

[8] D. Wang, B. Zhang, C. Guo, B. Gao, J. Wang, G. Yang, H. Huang, F. Nie, Formulation and Performance of Functional Sub-micro CL-20-based Energetic Polymer Composite Ink for Direct-write Assembly, *RSC Adv.* **2016**, *6*, 112325–112331.

[9] A. C. Ihnen, A. M. Petrock, T. Chou, P. J. Samuels, B. E. Fuchs, W. Y. Lee, Crystal Morphology Variation in Inkjet-Printed Organic Materials, *Appl. Surf. Sci.* **2011**, *258*, 827–833.

[10] A. C. Ihnen, A. M. Petrock, T. Chou, B. E. Fuchs, W. Y. Lee, Organic Nanocomposite Structure Tailored by Controlling Droplet Coalescence during Inkjet Printing, *ACS Appl. Mater. Interfaces* **2012**, *4*, 4691–4699

[11] J. Wang, C. Xu, C. An, C. Song, B. Liu, B. Wu, X. Geng, Preparation and Properties of CL-20 based Composite by Direct Ink Writing, *Propellants Explos. Pyrotech.* **2017**, *42*, 1139–1142.

[12] S. K. Bhattacharia, A. Maiti, R. H. Gee, J. Nunley, B. L. Weeks, Effect of Homolog Doping on Surface Morphology and Mass Loss Rates from PETN Crystals: Studies using Atomic Force Microscope and Thermogravimetric Analysis, *Propellants Explos. Pyrotech.* **2014**, *39*, 24–29.

[13] A. A. Kotomin, A. S. Kozlov, V. V. Gorovtsov, V. V. Efanov, M. A. Trapeznikov, S. A. Dushenok, E. N. Breshev, Regulation of Detonation Ability of Explosive Materials Used in Spacecraft Separation Systems, *Solar Syst. Res.* **2012**, *46*, 511–518.

[14] V. Shahedifar, H. R. Tajik, A. M. Rezadoust, Studying the Thermal Properties of a Cotton/Epoxy Composite Inhibitor, *Propellants Explos. Pyrotech.* **2012**, *37*, 569–574.

[15] A. Elbeih, J. Pachman, S. Zeman, W. A. Trzcinski, M. Suceska, Study of Plastic Explosives based on Attractive Cyclic Nitramines, Part II. Detonation Characteristics of Explosives with Polyfluorinated Binders, *Propellants Explos. Pyrotech.* **2013**, *38*, 238–243.

[16] O. A. Nafday, R. Pitchimani, B. L. Weeks, Patterning High Explosives at the Nanoscale, *Propellants, Explos. Pyrotech.* **2006**, *31*, 376–381.

[17] Y. Ou, *Explosives*, Vol. 7, Beijing Institute of Technology Press, Beijing, **2014**, pp. 268-270.

[18] D. Wang, B. Gao, G. Yang, F. D. Nie, H. Huang, Preparation of CL-20 Explosive Nanoparticles and Their Thermal Decomposition Property, *J. Nanomater.* **2016**, *38*, 5462097.
[19] H. E. Kissinger, Reaction Kinetics in Differential Thermal Analysis, *Anal. Chem.* **1957**, *29*, 1702–1706.
[20] T. Ozawa, A New Method of Analyzing Thermogravimetric Data, *Bull. Chem. Soc. Jpn.* **1965**, *38*, 1881–1886.
[21] P. G. Boswell, On the Calculation of Activation Energies Using Modified Kissinger Method, *J. Therm. Anal.* **1980**, *18*, 353–358.
[22] T. Zhang, R. Hu, Y. Xie, F. Li, The Estimation of Critical Temperatures of Thermal Explosion for Energetic Materials Using Non-isothermal DSC, *Thermochim. Acta* **1994**, *244*, 171–176.
[23] M. Li, L. Lan, H. Pang, M. Wen, S. Jing, Measurement of PBX Elastic Modulus by Nano-indentation, *Chin. J. Energ. Mater.* **2007**, *15*, 101–104.
[24] C. Leiber, *Assessment of Safety and Risk with a Microscopic Model of Detonation*, Vol. XXIII, Elsevier, Amsterdam, **2003**, pp. 520-521.
[25] Y. Wei, J. Wang, C. An, H. Li, X. Wen, B. Yu, GAP/CL-20-Based Compound Explosive: A New Booster Formulation Used in a Small-Sized Initiation Network, *J. Energ. Mater.* **2017**, *35*, 53–62.

Received: March 4, 2018
Revised: September 5, 2018
Published online: October 10, 2018

